Soft Failure Identification for Long-haul Optical Communication Systems Based on One-dimensional Convolutional Neural Network

Huazhi Lun, Mengfan Fu, Xiaomin Liu, Yiwen Wu, Lilin Yi, Weisheng Hu, and Qunbi Zhuge

***Abstract*—With the advance of elastic optical networks, optical communication systems are becoming more flexible and dynamic. In this scenario, soft failures are more likely to occur due to various link impairments. If these soft failures are not handled properly and timely, service disruption may occur. Identifying the cause of soft failure is a key step to restore the degraded links. However, it is difficult for traditional methods to accomplish this task. Fortunately, powerful machine learning (ML) algorithms provide a promising path to address this problem. In this article, a novel two-stage soft failure identification scheme based on a convolutional neural network (CNN) and receiver DSP is proposed. The input of the CNN is the power spectrum density (PSD) extracted from a coherent receiver, and the output contains the identified cause of soft failures together with their probabilities. Extensive simulations are performed to validate the proposed method. Four types of soft failure causes are explored including the offset of optical filter's center frequency (FS), the tightening of optical filter's 3-dB bandwidth (FT), SNR degradation due to the increased amplified spontaneous emission (ASE) noise, and the Kerr nonlinear effect. When only one soft failure cause exists, excellent accuracy is achieved. When multiple soft failure causes exist, the probabilities of these causes provided by the CNN are used to gain insight into their influences on the system. Finally, we investigate the interpretation of the CNN and a reasonable interpretation is given and discussed.**

***Index Terms*—Failure identification, soft failure, coherent receiver, digital signal processing, convolutional neural network.**

I. Introduction

With the rapid progress of 5G, the internet of things, cloud computing, and high definition video, the demand for the capacity of optical networks is dramatically increasing. To meet such high a demand, the architecture of optical systems is evolving towards more dynamic and intelligent. In particular, the design of low margin optical networks is attracting increasing attention. In this scenario, soft failures are more likely to occur due to different kinds of link impairments. These soft failures may lead to service disruption if not handled timely and accurately. Therefore, it is essential to fix the soft failure once it is detected. During this process, identifying the cause of the soft failure is quite crucial. However, for traditional methods based on mathematical models, it is difficult to get an analytic formula to obtain the cause of the soft failure. Fortunately, the fast-growing machine learning methods provide a promising path to address this problem, and many relevant works have been reported. In [1], [2], bit error rate (BER) is monitored, and the characteristics of it are analyzed and input to a neural network to identify the soft failure cause between wavelength selective switch (WSS) and amplified spontaneous emission (ASE) noise. One shortcoming of this method is that the required time window for monitoring the trend of BER is long, and when the monitoring window is five minutes, the accuracy can achieve 91%. In [3], [4], an optical spectrum analyzer (OSA) is used to obtain the optical spectrum of signals to identify the soft failure caused by filter shift (FS) or filter tightening (FT). Although the accuracy can achieve 100%, the use of OSA may increase the cost of the system. The features are manually selected, and it may take great efforts to obtain optimum characteristics to achieve the best performance. Besides, the theoretical spectrum of the signal is needed. It has to be calculated in the controller, leading to an increase of its burden. In [5], a finite state machine (FSM) is utilized to detect the degradation of BER and to identify the corresponding cause between FT and laser drift. However, the accuracy of the algorithm is highly dependent on the proper configuration of the parameters of the algorithm. Since the optical links are heterogeneous, it can be challenging to find the optimum configuration of these parameters.

The methods mentioned above all ignore fiber nonlinear impairments (NLI). Since receiver DSP can compensate for chromatic dispersion (CD) and polarization mode dispersion, the soft failures in a link are mainly caused by ASE noise, WSS filtering effect, and fiber NLI. Therefore, NLI is also a vital soft failure cause that should be considered. Also, some algorithms [1], [3], [4] need intermediate link information, which may cause exploding data transfer between the controller layer and the physical layer. Besides, to obtain these intermediate information, additional devices are needed, increasing the cost of implementation. Finally, most algorithms do not consider the scenario when multiple types of soft failures occur. In this case, it is essential to understand their respective influences on the

Manuscript received December 1, 2019; revised March 9, 2020 and April 16, 2020; accepted April 17, 2020. Date of publication April 20, 2020; date of current version May 27, 2020. This work was supported in part by the National Natural Science Foundation of China under Grant 61801291, in part by the Shanghai Rising-Star Program under Grant 19QA1404600, and in part by the National Key R&D Program of China under Grant 2018YFB1801203. *(Corresponding author: Qunbi Zhuge.)*

The authors are with the State Key Laboratory of Advanced Optical Communication Systems and Networks, Shanghai Institute for Advanced Communication and Data Science, Shanghai Jiao Tong University, Shanghai 200240, People's Republic of China. (e-mail: huazhi.lun.sjtu@gmail.com; mengfan.fu@sjtu.edu.cn; xiaomin.liu@sjtu.edu.cn; evanwu@sjtu.edu.cn; lilinyi@sjtu.edu.cn; wsh@sjtu.edu.cn; qunbi.zhuge@sjtu.edu.cn).

Color versions of one or more of the figures in this article are available online at https://ieeexplore.ieee.org.

Digital Object Identifier 10.1109/JLT.2020.2989153

system. To achieve this, the information of each soft failure is needed to gain insight into the state of the link.

To address the problems above, we have proposed and presented a receiver DSP aided soft failure identification scheme in the European Conference on Optical Communication (ECOC) [6]. In this paper, we extend the previous work and improve the architecture of the proposed method. A novel two-stage soft failure identification algorithm based on a convolutional neural network (CNN) and receiver DSP is proposed and validated. Compared with our previous work, the architecture of the CNN can be much simpler thanks to the two-stage design. The parameter numbers of the previous method are 25872, and the parameter numbers of the improved two-stage method in this paper are 3960, which are just 15.3% of the pervious method without any performance degeneration. The simpler architecture of the proposed method making the algorithm more robust against overfitting and outlier. The power spectrum density (PSD) of received signals is used as the input of the CNN, which can be easily obtained from a coherent receiver using a fast Fourier transform (FFT) [6]. Since no additional devices are needed in the proposed scheme, it is possible to achieve a low-cost implementation. Besides, the use of the CNN enables the algorithm to skip the complex process of feature extraction (also called feature engineering) by finding optimum features automatically. Finally, to deal with the case that multiple types of soft failures exist, the probability information of each impairment is output to help understand and identify the multiple soft failure causes simultaneously in a system.

In this paper, the WSS filtering impairments, i.e., FS and FT, ASE noise, and fiber NLI are all considered. To validate the proposed scheme, extensive simulations are performed, and the results demonstrate high accuracy and superior generalization performance. Furthermore, instead of treating the CNN as a black box, we provide an explanation on the mechanism of the CNN using the method described in [7].

This paper is organized as follows. Section II explores the characteristics of the signal's PSD in different soft failure scenarios. Based on the analysis, we propose to use a one-dimensional CNN to extract information from the PSD to address the identification problem. The basic architecture of the CNN and the overall framework of the proposed method are then introduced. In Section III, we describe the simulation setup in detail. In this section, we describe the process of generating data for training and testing the CNN as well as the architecture of the adopted CNN. In Section IV, we present and discuss the performance of the proposed scheme. The results demonstrate superior accuracy and good generalization performance. The paper is concluded in Section V.

II. Principle

A. Theoretical Analysis

To identify the cause of the soft failure in a fiber link, it is crucial to obtain information about the status of the system. This can be achieved by analyzing the optical spectrum of the signal in the intermediate nodes of a link using OSA, as described in [2]. However, this will increase system cost. Alternatively, the electrical PSD of a signal also reflects the overall status of the link and can be used to realize the soft failure identification function. Note that the electrical PSD of a signal can be easily obtained from receiver DSP using FFT.

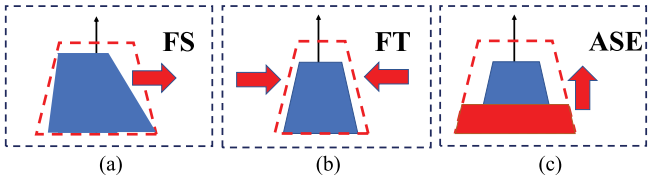

Fig. 1. (a) Illustration of FS, (b) FT and (c) increased ASE noise.

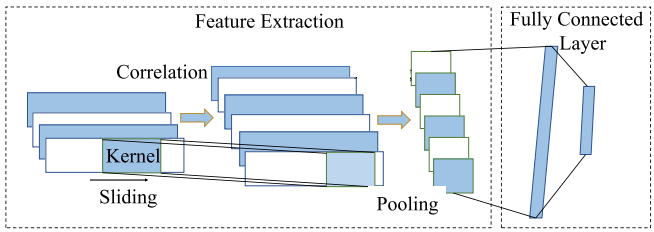

Fig. 2. A typical architecture of a one-dimensional CNN.

Fig. 1(a), (b), and (c) show the PSD of a signal when the FS, FT, and increased ASE noise occur, respectively. It can be seen from the figure that, if the FS occurs, one edge of the signal is filtered, but the other side is retained, leading to the destruction of the symmetry. If the FT occurs, the symmetry of the PSD is held, but the edge of the PSD is much sharper than the normal one. If the ASE noise is increased, the shape of the PSD remains unchanged, but the noise floor becomes higher. Finally, if the soft failure is caused by the fiber nonlinear effect, the shape of the PSD is not changed, but a special correlation will be introduced into the PSD due to the interaction between the CD and NLI [8].

Therefore, when different types of soft failures occur, the PSD will exhibit different characteristics, which makes it possible to identify the cause of the soft failure by analyzing it. However, it is difficult to analyze the PSD using traditional analytic methods, i.e., deriving a formula to obtain the cause of the soft failure from the PSD. Instead, methods based on deep learning can be adopted. Inspired by the great success achieved by CNN in image classification due to its powerful capability to extract spatial correlation between the pixels of an image, we adopt a one-dimensional CNN to extract useful information from the PSD to identify the soft failure cause.

B. One-dimensional Convolutional Neural Network

A typical architecture of a one-dimensional CNN is shown in Fig. 2. It is composed of several convolutional layers and pooling layers. The last layer of CNN is usually fully connected. The convolutional layer is responsible for feature extraction. In this layer, a correlation operation is conducted between the PSD of the signal and a sliding window called kernel with trainable parameters. The convolutional process can be expressed as $y_i = f(\Sigma_k \Sigma_j x_{i-j,k} w_{j,k} + b_k)$, where x, y, and w represent

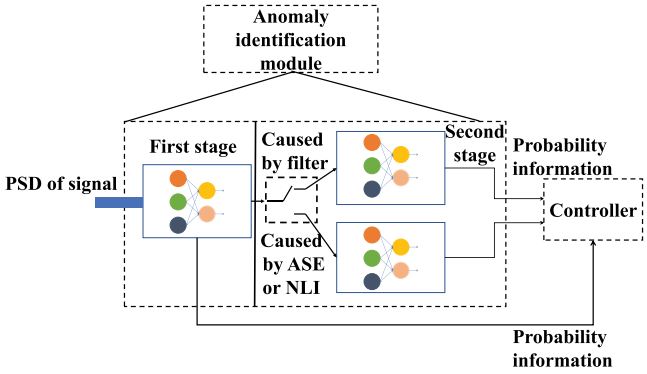

Fig. 3. The two-stage operation of the proposed method.

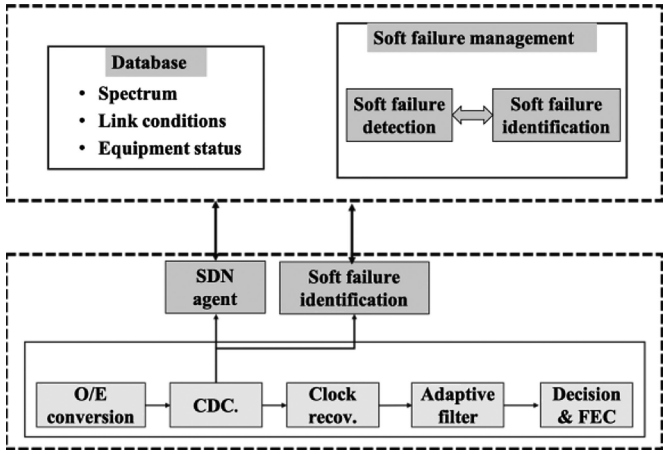

Fig. 4. The architecture of the proposed scheme.

the PSD, the output of the convolutional layer, and the trainable parameters of the kernel, respectively. The subscript i and j represent the indices of the input tensor, and they are integer values. The subscript k represents the k-th channel.

Following the convolutional layer, pooling operations are conducted, and the max-pooling operation is employed in this work. In this layer, a window slides along the signal with a fixed stride, and only the maximum value in the window is preserved. Afterwards, a fully connected layer is applied, and the output is mapped into probability distributions using the expression $P_i = \exp(y_i) / \Sigma_j exp(y_j)$, where y_i represents the i-th output of the fully connected layer. The one with a maximum probability among the candidates of the soft failure causes will be identified as the dominant cause. Because the probability information is obtained, the secondary cause can also be identified in the proposed method, which is useful when multiple soft failures co-exist.

C. The Framework of the Proposed Scheme

A CNN is embedded in the soft failure identification module. The cause of soft failure can be classified into two subgroups according to whether it is caused by WSS or not. Therefore, it is natural to divide the identification process into two stages, as shown in Fig. 3.

The first stage is responsible for identifying whether WSS causes the soft failure. If it determines that the WSS filtering effect causes the soft failure, the second stage will further identify whether the soft failure is caused by FS or FT. If the first stage decides that WSS does not cause the soft failure, the second stage will then identify whether the soft failure is caused by NLI or increased ASE noise. The two stages will both provide probability information for each soft failure cause. From the probability information, the dominant soft failure cause and the secondary soft failure cause can be easily determined.

The architecture of the proposed method based on the CNN described in the previous section is shown in Fig. 4.

A controller continuously monitors the physical layer. Once the soft failure detection module detects a soft failure, a notification will be sent to the soft failure identification module and the identification process will be performed afterwards. In this process, the PSD of the signal is first transferred from the receiver DSP to the soft failure identification module through a database, followed by the CNN calculation. The final identification results will be sent to the soft failure management module, and proper actions will be taken to restore the optical link. Because the features are extracted from the digital chromatic dispersion compensation module, the identification algorithm can be easily implemented in a coherent receiver especially when a programmable AI chip exists in the receiver. We can also adopt a hybrid approach. The first stage can be deployed in the receiver, which is just responsible for determining whether the soft failure is caused by WSS or not. The more sophisticated second stage can be deployed in the central controller. Another approach is to deploy the entire algorithm in the controller. In practice, the way of deployment depends on the co-design of local and global intelligence considering response speed and implementation complexity.

The performance of the proposed scheme will be discussed in the following section.

III. Simulation Setup and Results

A. Simulation Setup and the Architecture of the CNN

To obtain sufficient samples for the training and testing of the neural network, extensive simulations are performed. The simulation setup is shown in Fig. 5. At the transmitter side, a DP-16QAM signal is generated with a length of 2^{16} symbols. The symbol rate is set to 35 GBaud. A root-raised-cosine (RRC) filter is used for pulse shaping with a roll-off factor of 0.1. Laser phase noise is ignored in our study. The launch power is set to 0 dBm, which is the optimum power of the simulated scenario in this work. The link consists of 11 spans of 80 km standard single-mode fiber (SSMF) and is simulated using the split-step Fourier method (SSFM). To guarantee the accuracy of the SSFM, a constant step size of 20 m [9] is used. An Erbium-doped fiber amplifier (EDFA) with a noise figure of 5 dB is added at the end of each span to compensate for the loss of fiber completely. One WSS is inserted after the EDFA for every two spans, and the transfer function of a WSS is simulated using

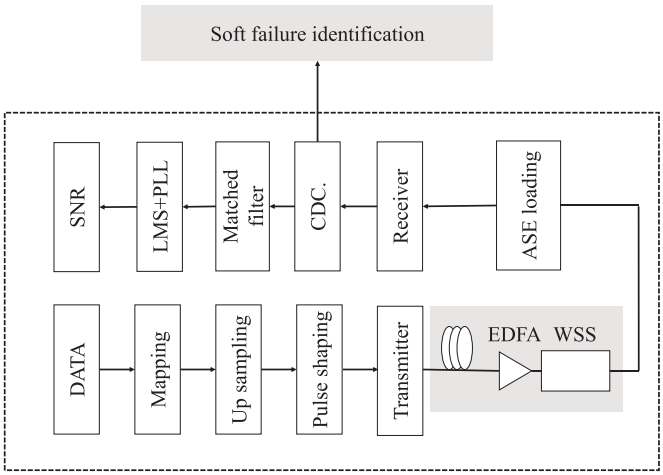

Fig. 5. Simulation setup.

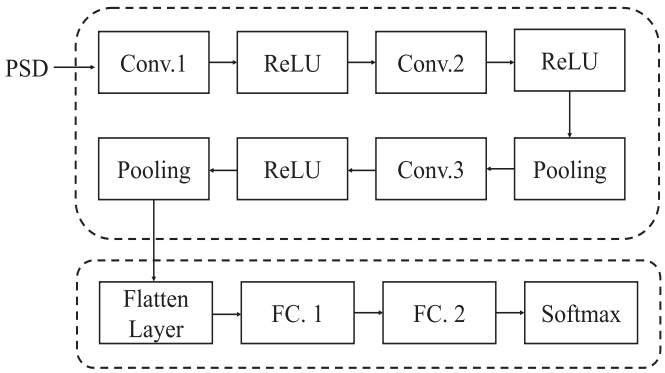

Fig. 6. The architecture of the adopted CNN.

the following equations:

$$S(f) = \frac{1}{2}\sigma\sqrt{2\pi}\left[erf\frac{(B_0/2 - f)}{\sqrt{2}\sigma} - erf\frac{(-B_0/2 - f)}{\sqrt{2}\sigma}\right] \quad (1)$$

$$\sigma = \frac{B_{OTF}}{2\sqrt{2\ln 2}} \quad (2)$$

where B_0 represents the bandwidth of the WSS, f represents the frequency, and the B_{otf} represents the steepness of the edge of the transfer function. At the receiver, the CD compensation and matched filter are first applied. After that, a least-mean-square (LMS) based adaptive filter is used to equalize the signal followed by a phase-locked loop (PLL) to implement the phase recovery. Finally, the signal-to-noise ratio (SNR) and the BER are calculated. Note that the ASE noise is loaded in the intermediate EDFA for the cases with abnormal FS, FT, and NLI. For the soft failure caused by the increased ASE noise, all the ASE noise is added at the receiver side.

The configurations of the adopted CNN for the first and second stages are shown in Fig. 6. The number of the points of the PSD is 2048. The kernel length and the number of the output channels of the first convolutional layer are 10 and 8, respectively. The number of the output channels of the second and third convolutional layers is 16 with a kernel length of 10. The stride of all convolutional layers is 1. For the two pooling layers, the sizes are 8 and 16, respectively. The strides are also 8 and 16, respectively. After the last convolutional layer, the output is flattened, followed by two fully connected layers. Dropout with probability equal to 0.5 is used to avoid overfitting between the two FC layers. In this work, the activation function is the rectified linear unit (ReLU) function.

TABLE I
SAMPLES GENERATED FOR THE TRAINING OF THE CNN

Soft failure type	Description
FS	The center frequency of each WSS is swept from -5 GHz to -18 GHz and 5 GHz to 18 GHz with a step size of 0.2 GHz.
FT	The 3-dB bandwidth of the WSS is swept from 19 GHz to 36 GHz with a step size of 0.2 GHz.
ASE noise	The value of SNR_{ASE} is swept from 6 dB to 9 dB with a step size of 0.01 dB.
NLI	The launch power is swept from 6 dBm to 9 dBm with a step size of 0.01 dB.

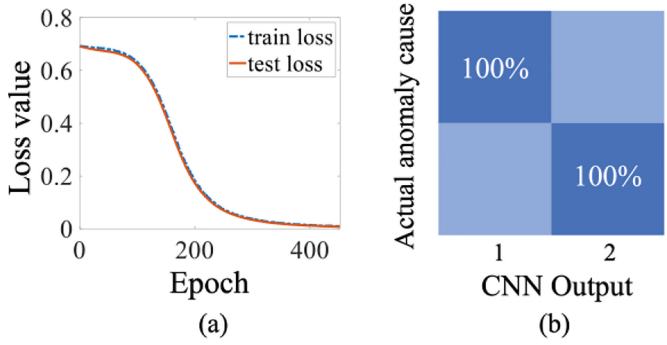

Fig. 7. (a) The learning curve of the CNN in Stage I and (b) the confusion matrix of Stage I.

B. Results and Discussions

1) The Identification Results for Single Soft Failure: To train and test the CNN, a sufficient number of samples are first generated. Since the probability of the situation that multiple WSS's are abnormal is low in practical systems, we assume only one WSS is in the abnormal state in our simulations. Note that when one type of soft failure is simulated, all the other conditions are set to their optimum values. The simulated scenarios are summarized in Table I.

The dataset consists of 1425 samples, and it is divided into the training set (80%) and the testing set (20%). The loss curves on the training and testing sets of the first stage are shown in Fig. 7(a). It can be observed that the CNN has converged, and no overfitting occurs during the training process. The identification accuracy of the first stage is shown in Fig. 7(b), where 1 represents the WSS filtering effects, and 2 represents the NLI or ASE noise. It can be seen that all soft failure causes are correctly identified. For the second stage, the loss curve is similar to the first stage, and the accuracy of the second stage also reaches

TABLE II
THE ACCURACY OF THE PROPOSED SCHEME IN DIFFERENT SCENARIOS

Modulation format	Distance (km)	Accuracy of the first stage	Accuracy of the final output
DP-QPSK	800	97%	97%
	960	98%	96%
	1120	100%	100%
DP-8QAM	800	98%	98%
	960	100%	100%
	1120	98%	98%
DP-32QAM	800	98%	96 %
	960	100%	100%
	1120	100%	100%

100%. To summarize, the accuracy of the proposed method can reach 100% when there exists only one type of soft failure.

2) The Generalization Performance: To test the generalization performance of the proposed scheme in different scenarios, we further simulate the following scenes. Note that the neural network did not see any of these new data during the training process. We simulate additional three modulation formats including DP-QPSK, DP-8QAM, and DP-32QAM. For each modulation format, we simulate its propagation over three links with lengths of 800 km, 960 km, and 1120 km. The roll-off factor of these new data is set to 0.02, the B_{OTF} of DP-QPSK, DP-8QAM, and DP-32QAM systems are set to 9.8 GHz, 7.8 GHz, and 6.8 GHz, respectively.

For each length, the locations of the WSS's are randomly distributed. To simulate the FS, the center frequency of each WSS is swept from 10 GHz to 18 GHz with a step size of 0.2 GHz. To simulate the FT, the 3-dB bandwidth of each WSS is swept from 19 GHz to 27 GHz with a step size of 0.2 GHz. To simulate the NLI, the launch power is swept from 6 dBm to 9 dBm with a step size of 0.01 dB. To simulate the ASE noise, the SNR_{ASE} is swept from 6 dB to 9 dB with a step size of 0.01 dB. The accuracy results are summarized in Table II. It can be concluded from the table that although these new data are never seen by the CNN, the results are still accurate, indicating a good generalization performance of the proposed method.

3) The Identification Results for Multiple Soft Failures: In practice, multiple soft failures may co-exist. In this work we focus on the scenario where two soft failures occur simultaneously. In this case, the proposed scheme needs to identify the dominant cause together with the secondary cause. To achieve this, we utilize the probability information in the output of the softmax function. To validate the performance, we simulate the case when two types among the four soft failures co-exist. The scenes with the FT and NLI/ASE are simulated first, and the configurations of the simulation setup are summarized in Table III.

When the FT and NLI both cause the soft failure, the probability information of the first stage and second stage is shown in Fig. 8. As shown in Fig. 8(a), in the first stage, the influence of the FT is more significant than the NLI when the filter bandwidth is small. As the bandwidth of the WSS increases, the probability

TABLE III
THE SIMULATION CONFIGURATION

Soft failure type	Description
FT and NLI	The 3-dB bandwidth of the first WSS is swept from 35 GHz to 42 GHz with a step size of 0.1 GHz. The launch power of the signal is set to 6.6 dBm.
FT and ASE noise	The 3-dB bandwidth of the first WSS is swept from 30 GHz to 40 GHz with a step size of 0.1 GHz. The SNR_{ASE} is set to 11 dB.

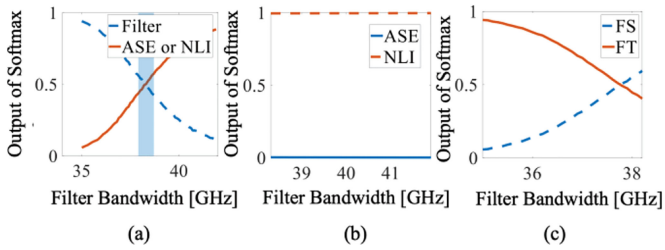

Fig. 8. (a) Probability results of the first stage. (b) Probability results for the classification of ASE noise and NLI. (c) Probability results for the classification of FS and FT.

of the NLI or ASE increases gradually. In the colored area of Fig. 8(a), the output values of the softmax for the two types of soft failures are similar, which means from the perspective of the CNN, the WSS filtering effect and NLI/ASE have a comparable influence on the system. Therefore, in this area, these two types of soft failure causes should be both checked to restore the link to a normal state.

As shown in Fig. 8(b), when the first stage identifies that the ASE noise or NLI causes the soft failure, the output of the second stage correctly identifies that the NLI causes the soft failure. When the first stage identifies that the WSS causes the soft failure, the identification results of the second stage are shown in Fig. 8(c). It can be seen from the figure that when the 3-dB bandwidth ranges from 37.8 GHz to 38.2 GHz, the results are incorrect. This frequency range corresponds exactly to the colored area in Fig. 8(a), in which the FT and NLI have a similar influence on the system. Therefore, the second stage has some difficulty in making the right judgments in this frequency range. However, in most cases, the output of the second stage is correct. Besides, in this range, the WSS and ASE/NLI should be checked simultaneously as described before. Since the second stage has correctly identified that part of the cause is NLI, once the NLI of the link is restored to the optimum state, there will exist only one soft failure in the link. In this case, as described in the previous subsection, the accuracy of the identification for the FS and FT is 100%.

Next, we test the case when the FT and increased ASE noise co-exist. The results are shown in Fig. 9. The first stage can figure out which is the dominant soft failure cause between the WSS and ASE/NLI. As the bandwidth increases, the influence of the WSS on the system decreases gradually. At the same time, the influence of the ASE/NLI increases gradually. In the second stage, if the ASE/NLI is determined as the dominant soft

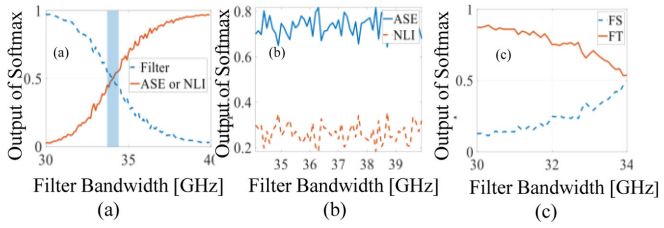

Fig. 9. (a) Probability results of the first stage. (b) Probability results for the classification of ASE noise and NLI. (c) Probability results for the classification of FS and FT.

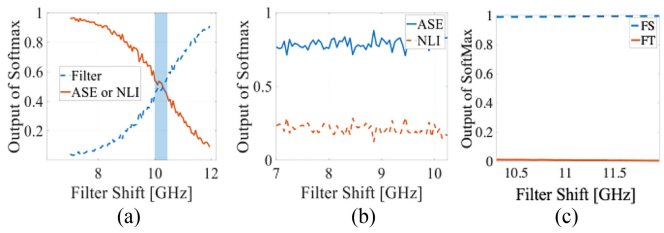

Fig. 11. (a) Probability results of the first stage. (b) Probability results for the classification of ASE noise and NLI. (c) Probability results for the classification of FS and FT.

TABLE IV
THE SIMULATION CONFIGURATION

Soft failure type	Description
FS and NLI	The FS value of the first WSS is swept from 7 GHz to 10 GHz with a step size of 0.05 GHz. The launch power is set to 6.6 dBm.
FS and ASE noise	The FS value of the first WSS is swept from 8 GHz to 12 GHz with a step size of 0.05 GHz. The SNR_{ASE} is set to 11 dB.

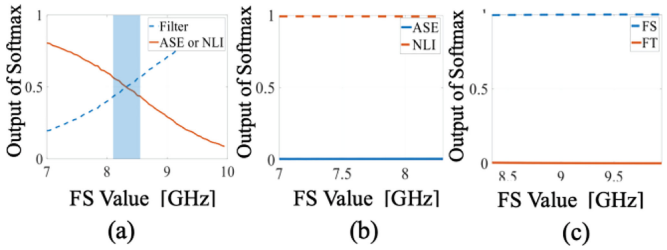

Fig. 10. (a) Probability results of the first stage. (b) Probability results for the classification of ASE noise and NLI. (c) Probability results for the classification of FS and FT.

failure cause, the outputs of the CNN responsible for identifying between the ASE noise and NLI are all correct, as shown in Fig. 9(b). However, if the WSS is determined as the dominant soft failure cause, the CNN responsible for identifying between the FS and FT seems to have some difficulties in making correct identification when the bandwidth is close to 34 GHz, as shown in Fig. 9(c). The reason behind this is the same as described in the previous scenario when the FT and NLI co-exist.

After that, the scenarios when the FS and ASE/NLI co-exist are simulated. The simulation configurations are summarized in Table IV.

The probability results when the FS and NLI co-exist are shown in Fig. 10. As shown in Fig. 10(a), in the first stage, as the FS increases, the probability of the WSS increases gradually. In the second stage, if the ASE/NLI is identified as the dominant cause, the CNN responsible for identifying between the ASE noise or NLI is accurate as shown in Fig. 10(b), and if the WSS is identified as the dominant cause, the CNN responsible for it also outputs all correct results as shown in Fig. 10(c).

Next, we test the case when the FS and ASE co-exist. The results are shown in Fig. 11 and they are similar to the results for the case when the FS and NLI noise co-exist.

TABLE V
THE SIMULATION CONFIGURATION

Soft failure type	Description
FS and FT	The launch power is set to the optimal value, and the SNR_{ASE} is set to the normal value. The FS value of the first WSS is set to 15 GHz. The bandwidth of the third WSS is swept from 24 GHz to 37 GHz with a step size of 0.1 GHz.
ASE noise and NLI	The launch power of the signal is set to 6.6 dBm. The SNR_{ASE} of the signal is swept from 12 dB to 18 dB with a step size of 0.1 dB.

To summarize, when the soft failure is caused by the WSS and the ASE/NLI, it is vital to understand the dominant cause of the soft failure. To achieve this, the probability output of the softmax function is utilized, from which their respective influences on the system can be easily obtained. One phenomenon noticed here is that the results of the second stage for the identification between the FS and FT are more accurate in the case when FS and ASE/NLI co-exist than the case when FT and ASE /NLI co-exist. This is because the influence of the FS on the shape of PSD is much bigger than the FT. Therefore, the identification of the FS is less influenced by other impairments than FT.

We then test the case when the soft failure is caused just by the WSS or ASE/NLI. The configuration of the simulation is summarized in Table V.

The case when the FS and FT co-exist is first tested. The results are shown in Fig. 12(a) and (b). In this case, the soft failure is only caused by the WSS. Therefore, the identification results of the first stage should always be the WSS. The results are shown in Fig. 12(a). In the second stage, with the decrease of the bandwidth, the probability of the FT increases gradually, which is also consistent with our expectation.

Finally, we test the case when the NLI and ASE noise co-exist. The results are shown in Fig. 13(a) and (b). In this case, the first stage's output should always determine that the ASE/NLI causes the soft failure. The result which is consistent with the expectation is shown in Fig. 13(a). The second stage's output is shown in Fig. 13(b). It can be seen that as expected the probability of the ASE noise increases gradually as SNR_{ASE} decreases.

To conclude, when multiple soft failures exist, the PSD will contain the characteristics caused by these soft failures. With the help of the probability information output by the softmax, the dominant soft failure cause can be identified. Once the dominant

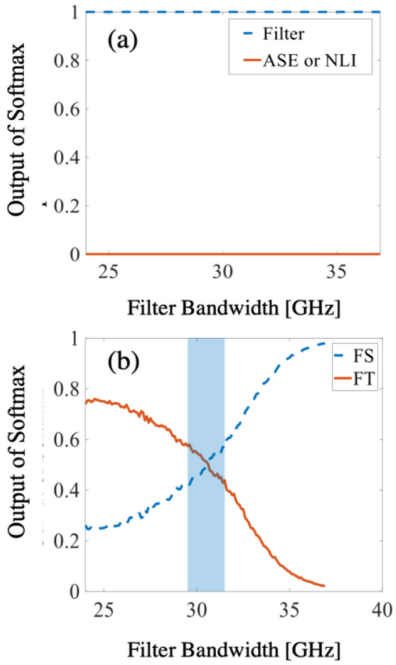

Fig. 12. (a) Probability results of the first stage. (b) Probability results for the classification of ASE noise and NLI.

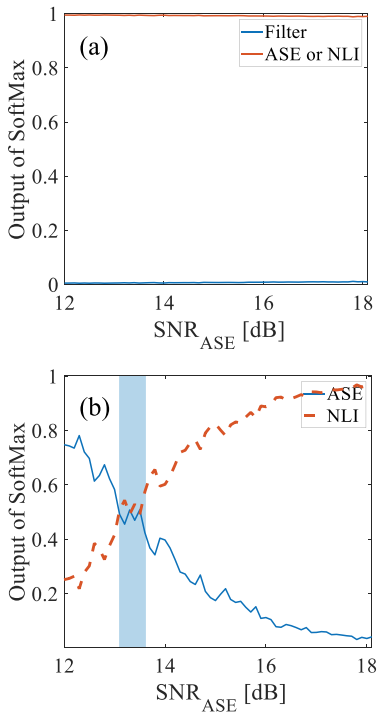

Fig. 13. (a) Probability results of the first stage. (b) Probability results for the classification of ASE noise and NLI.

one is solved, the second one will become the dominant one. By repeating the above process all soft failures can be addressed.

C. The Interpretation of the CNN

The accuracy and generalization performance of the trained CNN has been discussed and analyzed in the previous subsections. In this part, we provide an exploration of the mechanism

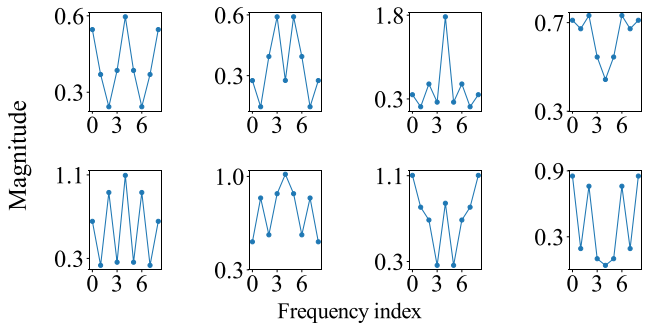

Fig. 14. The CNN kernels of the first stage in the frequency domain.

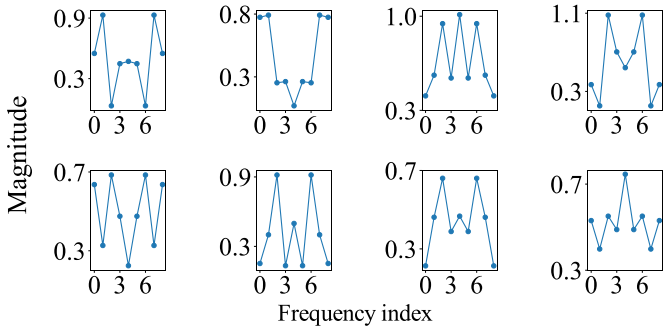

Fig. 15. The CNN kernels for the classification of FS and FT in the frequency domain.

behind it. The kernel of the CNN is quite similar to a finite impulse response (FIR) filter. Therefore, the interpretation of the CNN can be performed from the perspective of signal processing as described in [8]. To achieve this, we plot and analyze the kernel value of the first convolutional layer of the CNN.

We first analyze the kernel value of the first stage in the frequency domain. The kernel is transformed into the frequency domain using FFT, and the zero frequency is shifted to the center. Fig. 14 plots the resulted magnitude as a function of the frequency. It can be seen that some kernels are responsible for extracting the edge feature of the PSD such as the third kernel of the second row. Some kernels are responsible for extracting features from the center of the PSD such as the second kernel of the second row. Some kernels are responsible for extracting features from both the edge and the central part of the PSD such as the first kernel of the second row. Based on these extracted features, the CNN of the first stage can detect the features of the PSD and identify whether the soft failure is caused by WSS or not.

We then analyze the kernel values of the CNN of the second stage responsible for the identification between FS and FT. The kernel value is shown in Fig. 15. Similarly, different kernels are responsible for extracting features from different parts of the PSD. If FS causes the soft failure, the information extracted from different parts of the PSD can help detect the unsymmetrical feature of it. If FT causes the soft failure, the information extracted from the PSD can help the CNN detect the increased sharpness of the edge of the PSD. Therefore, with the extracted information, the CNN can identify whether the soft failure is caused by FS or FT.

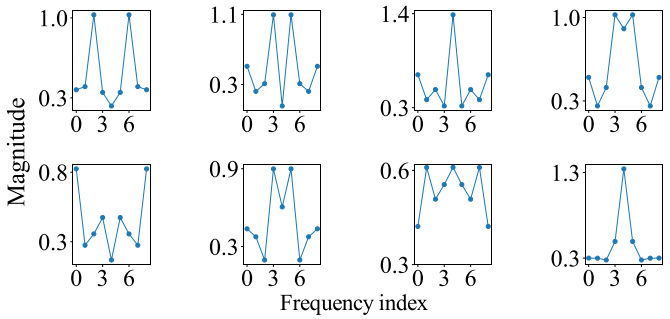

Fig. 16. The CNN kernels for the classification of NLI and ASE noise in the frequency domain.

Finally, in Fig. 16, we plot the kernel values of the CNN of the second stage responsible for the identification between NLI and ASE. It can be seen from the figure that some kernels are responsible for extracting the correlation information from the signal. Some kernels are responsible for extracting the information of the out-of-band ASE noise. If the ASE noise causes the soft failure, the information extracted from the out-of-band ASE noise can help the CNN identify it. If the soft failure is caused by the NLI, the special correlation will be detected, and NLI will be identified by the CNN.

To conclude, the kernel of the convolutional layer is similar to the FIR filter. It can extract information from different parts of the PSD. After analysis and synthesis, the CNN can identify the cause of the soft failure correctly.

IV. Conclusions

In this paper, we propose a two-stage soft failure identification scheme based on receiver DSP and CNN. By extracting features from the PSD of received signals, different soft failure causes can be identified. Through extensive simulations, we demonstrate the high accuracy and good generalization performance of the proposed scheme. In addition, instead of treating the adopted CNN as a black box, we explore the mechanism behind the CNN from the perspective of signal processing, and a reasonable explanation is provided.

References

[1] S. Shahkarami, F. Musumeci, F. Cugini, and M. Tornatore, "Machine learning-based soft-failure detection and identification in optical networks," in *Opt. Fiber Commun. Conf.*, San Diego, California, 2018, Paper M3A.5.

[2] F. Musumeci, C. Rottondi, G. Corani, S. Shahkarami, F. Cugini, and M. Tornatore, "A tutorial on machine learning for failure management in optical networks," *J. Light. Technol.*, vol. 37, no. 16, pp. 4125–4139, Aug. 2019.

[3] B. Shariati, M. Ruiz, J. Comellas, and L. Velasco, "Learning from the optical spectrum: failure detection and identification," *J. Light. Technol.*, vol. 37, no. 2, pp. 433–440, Jan. 2019.

[4] L. Velasco, B. Shariati, A. P. Vela, J. Comellas, and M. Ruiz, "Learning from the optical spectrum: soft-failure identification and localization [invited]," in *Opt. Fiber Commun. Conf.*, San Diego, California, 2018, Paper W1G.1.

[5] A. P. Vela *et al.*, "BER degradation detection and failure identification in elastic optical networks," *J. Light. Technol.*, vol. 35, no. 21, pp. 4595–4604, Nov. 2017.

[6] L. Velasco, B. Shariati, F. Boitier, P. Layec, and M. Ruiz, "Learning life cycle to speed up autonomic optical transmission and networking adoption," *J. Opt. Commun. Netw.*, vol. 11, no. 5, pp. 226–237, May 2019.

[7] H. Lun *et al.*, "Soft failure identification in optical networks based on convolutional neural network," in *Eur. Conf. Opt. Commun.*, Ireland, 2019, Paper P104.

[8] Z. Dong, F. N. Khan, Q. Sui, K. Zhong, C. Lu, and A. P. T. Lau, "Optical performance monitoring: a review of current and future technologies," *J. Light. Technol.*, vol. 34, no. 2, pp. 525–543, Jan. 2016.

[9] T. Tanimura, T. Hoshida, T. Kato, S. Watanabe, and H. Morikawa, "Convolutional neural network-based optical performance monitoring for optical transport networks," *J. Opt. Commun. Netw.*, vol. 11, no. 1, pp. A52–A59, Jan. 2019.

[10] Z. Wang, A. Yang, P. Guo, and P. He, "OSNR and nonlinear noise power estimation for optical fiber communication systems using lstm based deep learning technique," *Opt. Express*, vol. 26, no. 16, pp. 21346–21357, Aug. 2018.

[11] X. Chen, B. Li, R. Proietti, Z. Zhu, and S. J. B. Yoo, "Self-taught anomaly detection with hybrid unsupervised/supervised machine learning in optical networks," *J. Light. Technol.*, vol. 37, no. 7, pp. 1742–1749, Apr. 2019.

[12] S. Varughese, D. Lippiatt, T. Richter, S. Tibuleac, and S. E. Ralph, "Identification of soft failures in optical links using low complexity anomaly detection," in *Opt. Fiber Commun. Conf.*, San Diego, California, 2019, Paper W2A.46.

[13] Q. Zhuge *et al.*, "Application of machine learning in fiber nonlinearity modeling and monitoring for elastic optical networks," *J. Light. Technol.*, vol. 37, no. 13, pp. 3055–3063, Jul. 2019.

[14] D. Côté, "Using machine learning in communication networks [invited]," *J. Opt. Commun. Netw.*, vol. 10, no. 10, pp. D100–D109, Oct. 2018.

[15] F. N. Khan, Q. Fan, C. Lu, and A. P. T. Lau, "An optical communication's perspective on machine learning and its applications," *J. Light. Technol.*, vol. 37, no. 2, pp. 493–516, Jan. 2019.

[16] F. Musumeci, C. Rottondi, G. Corani, S. Shahkarami, F. Cugini, and M. Tornatore, "A tutorial on machine learning for failure management in optical networks," *J. Light. Technol.*, vol. 37, no. 16, pp. 4125–4139, Aug. 2019.

[17] Y. Pointurier, "Design of low-margin optical networks," in *Opt. Fiber Commun. Conf.*, San Diego, California, 2016, Paper Tu3F.5, 2016.

[18] J. Pesic, N. Rossi, and T. Zami, "Impact of margins evolution along ageing in elastic optical networks," *J. Light. Technol.*, vol. 37, no. 16, pp. 4081–4089, Aug. 2019.

[19] I. Sartzetakis, K. Christodoulopoulos, and E. Varvarigos, "QoT aware adaptive elastic optical networks," in *Opt. Fiber Commun. Conf.*, Los Angeles, California, 2017, Paper W4F.4.

[20] P. Soumplis, K. Christodoulopoulos, M. Quagliotti, A. Pagano, and E. Varvarigos, "Network planning with actual margins," *J. Light. Technol.*, vol. 35, no. 23, pp. 5105–5120, Dec. 2017.

[21] B. Shariati, M. Ruiz, and L. Velasco, "Out-of-field generic ML training with in-field specific adaptation to facilitate ML deployments," in *Opt. Fiber Commun. Conf. 2019*, San Diego, California, 2019, Paper Tu2E.3.